Chapter 4

Design of a Time-Domain Optical Breast Imaging System

A comprehensive review of the literature detailed in Chapter 3 indicated that no other clinical-ready time-domain mammographic optical imaging system exists that is capable of acquiring three-dimensional image data within a two to three minute period with multiple wavelengths and high source and detector spatial resolution. The Time-Domain Optical Breast Imaging System detailed in this dissertation is matched in capability by no other system and offers a unique opportunity to advance the state-of-the-art in optical mammography.

A system-level functional block diagram of the Time-Domain Optical Breast Imaging System is shown in Figure 4.1. The Source Subassembly is comprised of a mode-locked pulsed Ti:Sapphire laser with it's associated water cooling and control electronics interfaced to a Source Fiber Multiplexer, which switches the laser output into one of 150 fibers in the Source Fiber Array Quick-Connect. A fiber bundle connects the Source Subassembly to the Probe Subassembly, which is comprised of Source and Detector Fiber Probe Plates configured in transmission geometry. Both probe plates have quick-release features to enable the co-registration of an X-ray image. A second fiber bundle connects the Probe Subassembly to the Detector Subassembly, which is comprised of an objective lens that images the array of detection fibers onto a time-gated, image-intensified charge coupled device camera (ICCD).

The unique Source Fiber Multiplexer, which allows for switching between fiber positions within 300 μsec, is many orders of magnitude faster than typical mechanical switching systems used by other groups. The system allows for hundreds of source fibers to be utilized if desired. The current embodiment of the system interfaces to a Ti:Sapphire laser with a wavelength range between 750 and 850 nm. Although not used in this system, another embodiment of the Multiplexer was developed that was capable of combining six independent laser diodes into one optical fiber. This version of the
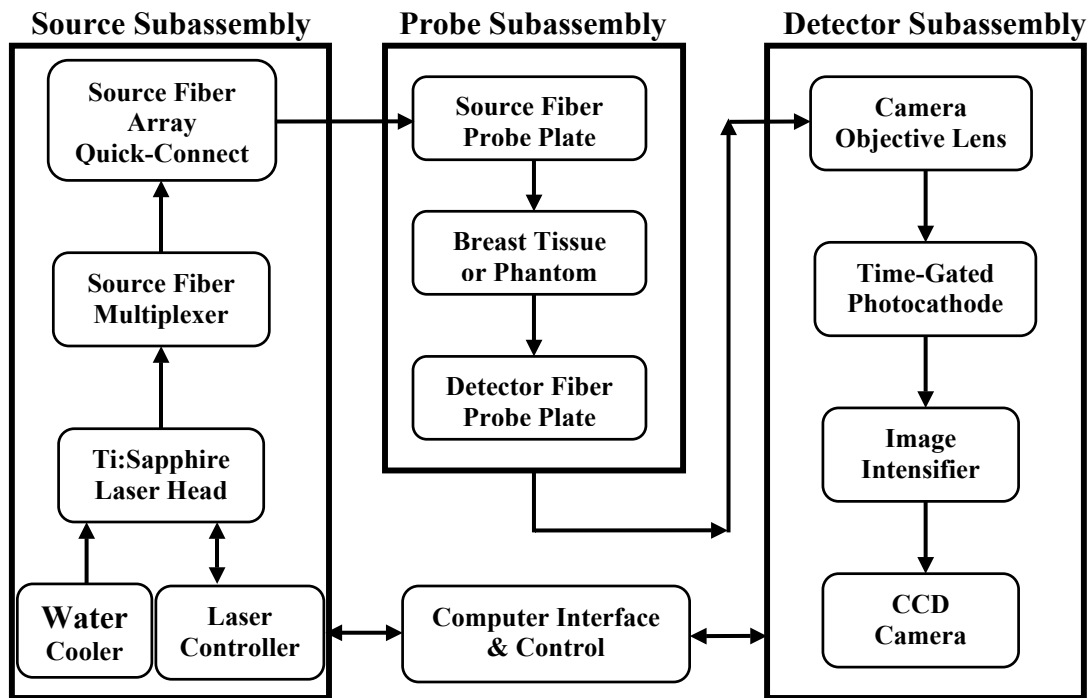
Figure 4.1   A system-level block diagram of the Time-Domain Optical Breast Imaging System is shown.

Multiplexer, which used the same scan engine design, could be used in future versions of the system, given suitable laser diode specifications.

The use of a fast, gated, image-intensified CCD camera (ICCD) allowed for data to be collected in parallel at discrete time delays, allowing complete TPSF's to be built up

for multiple source-detector positions. The third enabling feature of the system was the custom designed, high performance, unit magnification ICCD objective lens that permitted the massively parallel acquisition of 313 detection fibers.

The fourth enabling system feature was the compact source and detector fiber optic probe with unique quick-release features mounted within modified compression plates. The probe was designed to mate to a digital tomosynthesis X-ray mammography system to allow for co-registered multi-modality optical and X-ray images.

The details of the Time-Domain Optical Breast Imaging System are reviewed in the following sections. The first section discusses the system-level design and integration. The source subsystem is detailed next, followed by the detector subsystem and then the probe design. The last section reviews the design and fabrication of the homogeneous and heterogeneous phantoms and a Phantom Test Stand used to characterize the system in a laboratory setting.

4.1   System-Level Design of the Time-Domain Optical Breast Imaging System

The instrumentation for the Time-Domain Optical Breast Imaging System is shown in Figure 4.2, below. The fiber optic probe, which was a critically important part of the system, is not shown in the diagram. The probe is discussed in detail in Section 4.4.

The central thesis of this dissertation states that optical imaging of diffuse tissues must be combined in co-registration with a recognized gold standard of mammographic screening, i.e. X-ray mammography, to gain wide acceptance in the clinical environment. This multi-modality imaging approach promises to overcome the deficiencies of both imaging modalities by drawing on the strengths of each. Functional and structural image contrast would be provided by optical and high-resolution structural contrast by X-ray.

Furthermore, the structural information provided by the radiocontrast of X-ray could be used to improve the optical image reconstruction by providing boundary information and soft constraints for weakly correlated structural contrast. Ultimately, image-processing
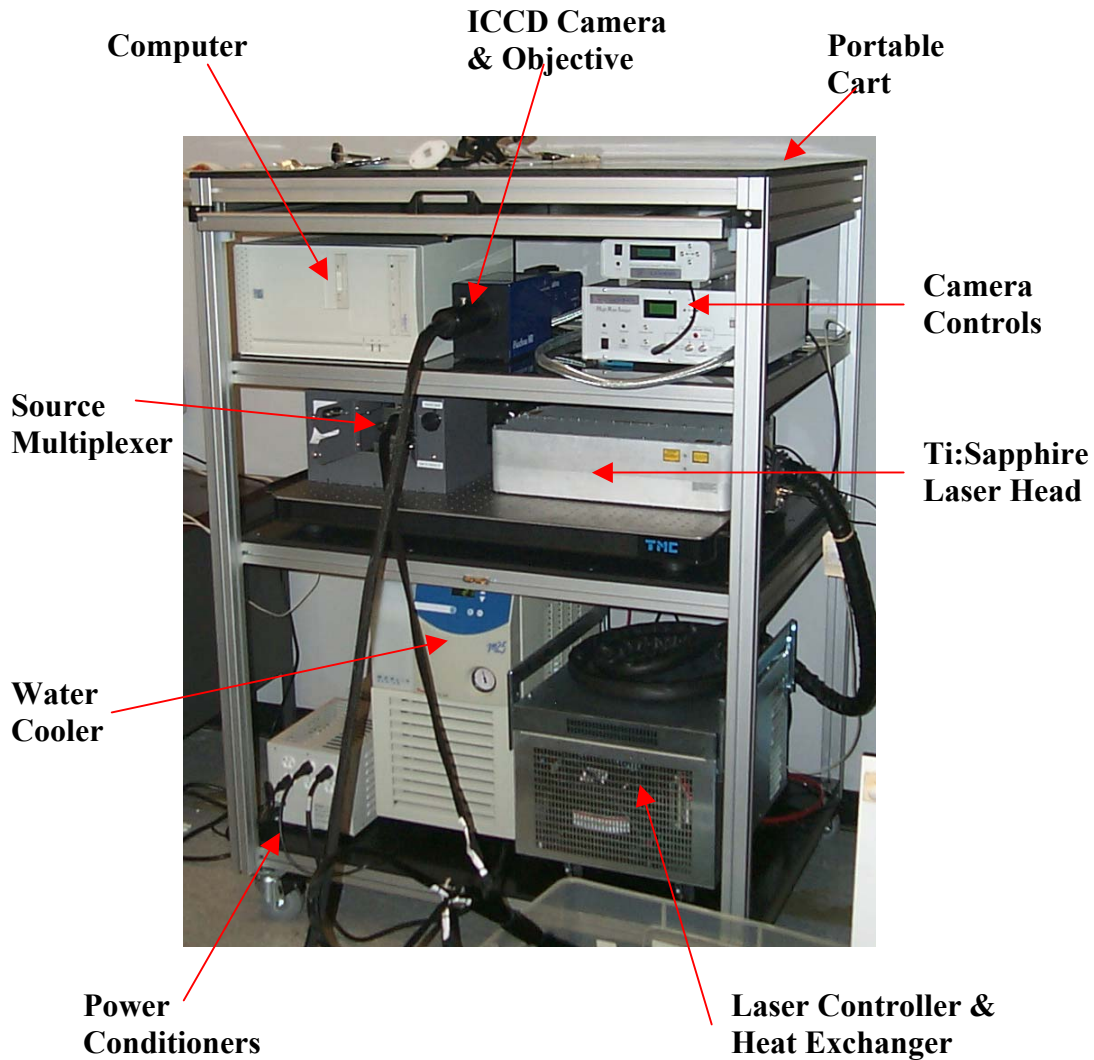
Figure 4.2   The Time-Domain Breast Imaging System instrument is shown housed in a wheeled cart. The probe is not shown.

techniques could be developed to provide the radiologist with a three-dimensional image indicative of both optical and X-ray contrast that would provide much greater information content than either modality alone.

With reference to Figure 4.2, all instrumentation for the Time-Domain Optical Breast Imaging System resided on a portable wheeled cart, with the exception of the probe, computer monitor, and keyboard. The lower shelf housed the power conditioning units on the left, the laser water cooler in the middle and the laser controller and heat exchanger on the right. The middle shelf held the Source Subassembly, consisting of the Source Fiber Multiplexer on the left and the Ti:Sapphire laser head on the right, both mounted on a sturdy optical bench. The bench was mounted on shock mounts to minimize shock and vibration that could have occurred during transportation. The laser head was attached to an umbilical containing electrical power and control lines and water-cooling hoses. The top shelf held the computer on the left, the ICCD camera system in the middle, connected to the probe by a black-jacketed fiber bundle, and the gate and image intensifier controllers on the right.

Software was written in the C language to provide for computer control of the laser and ICCD camera, data acquisition, data storage, and a user interface. The software was written and maintained by Jonathan Stott, Ph. D., of the Photon Migration Lab at Harvard's Massachusetts General Hospital. The Photon Migration Imaging (PMI) MatLab toolbox used for image reconstructions was primarily written by David Boas, Ph. D., Director of the Photon Migration Lab. Jonathan Stott was also responsible for many of the modifications to the toolbox for time-domain imaging.

4.2   Time-Domain Source Subsystem

The Time-Domain Source Subsystem is shown in rendered view in Figure 4.3. The laser head was the Mai-Tai mode-locked Ti:Sapphire laser diode pumped system from

Spectra Physics Corporation. It was modulated at 80 MHz and provided an average linearly polarized power between 700 and 1000 mW over the wavelength range between 750 and 850 nm. A synchronization pulse was provided out of the laser head to allow for precise control of the ICCD gate delay.

The output of the laser passed through a solenoid-activated safety shutter before entering the Source Fiber Multiplexer. The safety shutter was only open when the power

Fiber Source Multiplexer   **Safety Shutter**

Ti:Sapphire Laser Head

Quick-Connect Fiber Array Access Door

Intensity Adjustment

Portable Optical Table
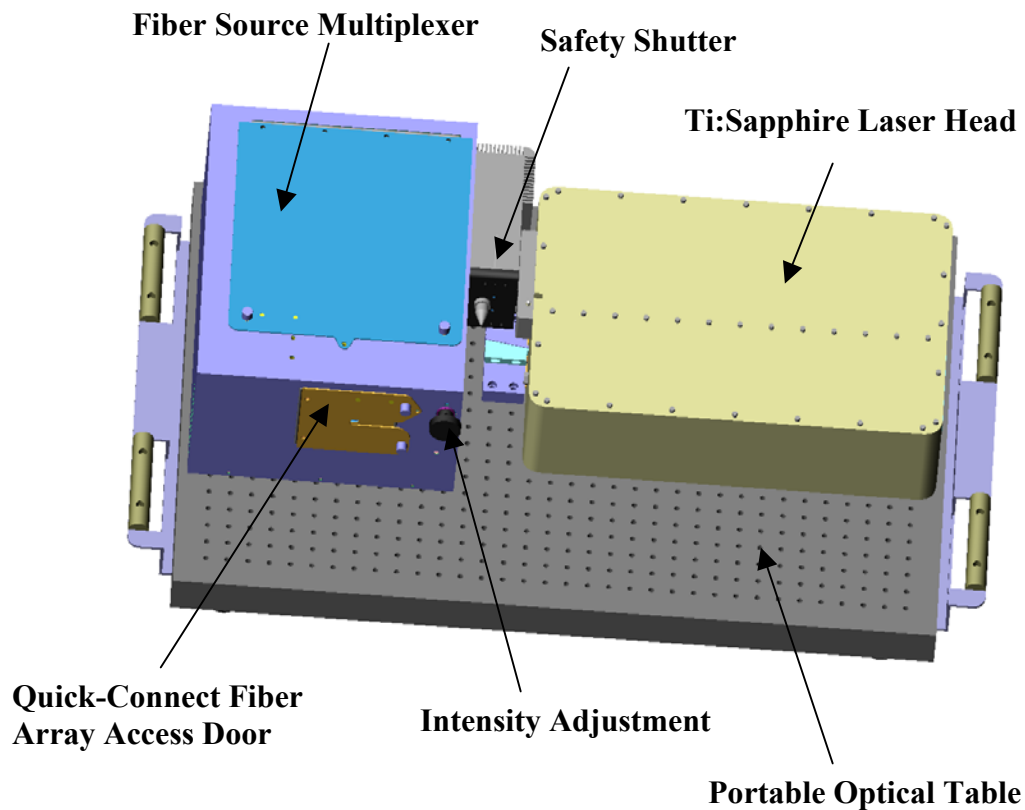
Figure 4.3   The laser source Assembly is shown in rendered view. The Mai-Tai Spectra Physics Ti:Sapphire laser head is shown on the right and the custom designed Source Fiber Multiplexer on the left. A safety shutter is shown as an interface between the two. Both devices were solidly mounted on top of an optical table.

was on and the top and front access doors were closed. There was also a switch on the front panel of the Multiplexer that allowed the shutter to be closed, even if all safety interlocks were engaged. The top door allowed for access to the galvanometers and

beam-attenuating polarizer without the need to remove the entire cover. The safety-

interlocked front access door was opened to insert or remove the Quick-Connect Source

Fiber Array, which was attached to the source probe. In the event that the Source Fiber

Array plug was not attached, a spring-loaded sliding door attached to the front access

Glan Calcite Polarizer for Laser Power Control

Fused Power Switch & Cooling Fan

Solenoid-Activated Safety Shutter

2-Axis Galvanometer

Power Supply & Galvanometer Control Boards

Telecentric Scan Lens

Kinematic Quick-Connect Fiber Array
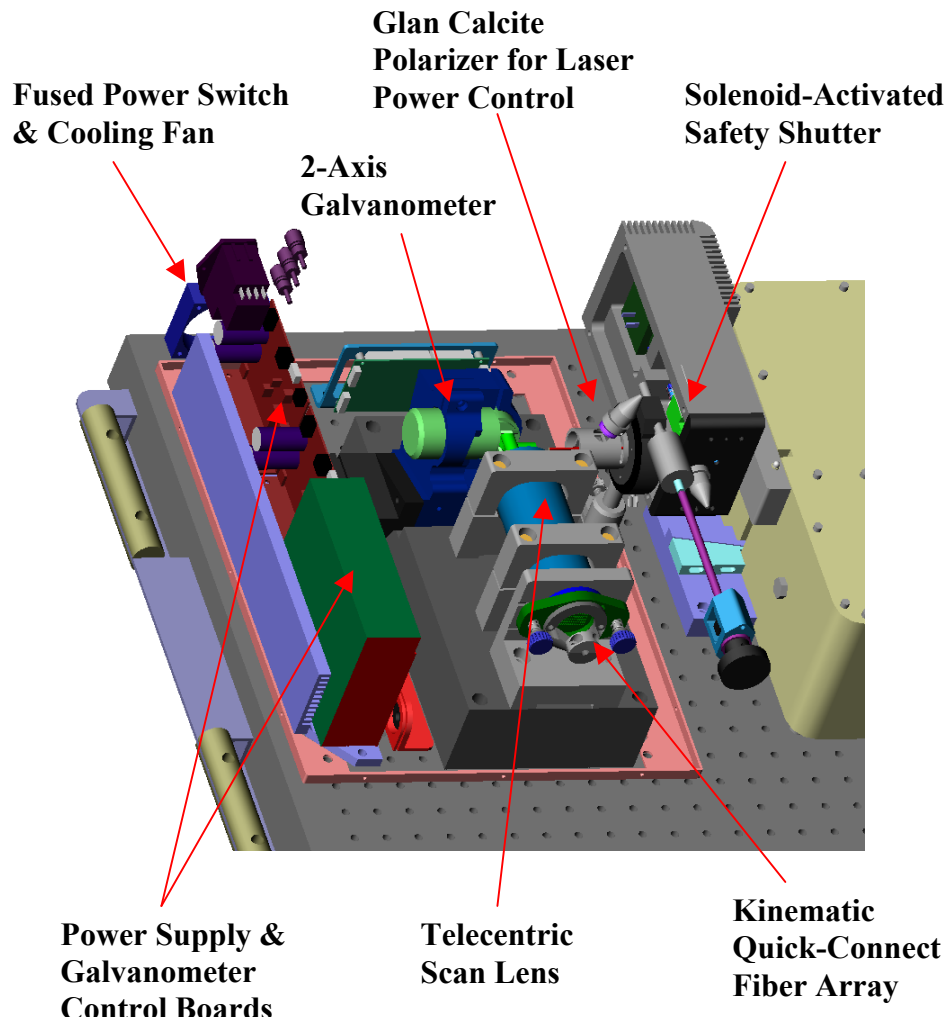
Figure 4.4   The components of the Fiber Source Multiplexer are shown in rendered view. The laser beam passes through the safety shutter to the rotating polarizer for power control. It is then steered by the 2-axis galvanometer into the telecentric f/θ scan lens that images the laser into one of 150 source fibers in the fiber array.

door closed to prevent laser emission from escaping when all safety interlocks were

engaged. The laser also had a clearly visible white LED on top of the laser head to

indicate emission from the laser. Additionally, the laser had a shutter built inside the laser head, which could be controlled by the user interface software routine.

A 10-turn knob was provided on the front panel of the Multiplexer to provide a 10x attenuation of the laser output, if desired. The knob caused a Glan Laser cube polarizer to rotate with respect to the linearly polarized output of the laser. The laser output was attenuated according to Malus's law, which decreases as the square of the cosine of the angle between the linear polarization axis of the laser output and that of the polarizing cube beamsplitter. The polarizer was attached to a precision rotation stage and had a beam dump to absorb power deviated by the polarizing beamsplitter as shown in Figure 4.4.

After passing through the polarizer assembly, the laser beam was deflected by a pair of galvanometers into the telecentric scan lens, which in turn focused the laser beam into one of 150 source fibers. The entire assembly was mounted on a solid aluminum base, which was attached to a rigid optical bench as indicated in Figure 4.3. No mirrors were used in the system other than the galvanometer mirrors to minimize alignment stability issues. The cover of the Multiplexer was compartmentalized to section off the optics from the power supply and galvanometer control boards. The power supply compartment had a cooling fan. The purpose of separating the compartments was to minimize the exposure of the optics to dust.

A close up of the Source Fiber Array Quick-Connect assembly is shown in Figure 4.5. The 150 fused silica source fibers had a core diameter of 200 μm and were plastic clad with a fluoropolymer providing a numerical aperture (NA) of 0.39. This numerical aperture was much higher than required by the very small image space NA of the

**Quick-Connect
Knobs**

**Fiber Bundle
Stain Relief**

**Alignment
Pins**

**Alignment
Balls**

**15 x 10 Array of
200 μm Fused
Silica Fibers of
0.39 NA**
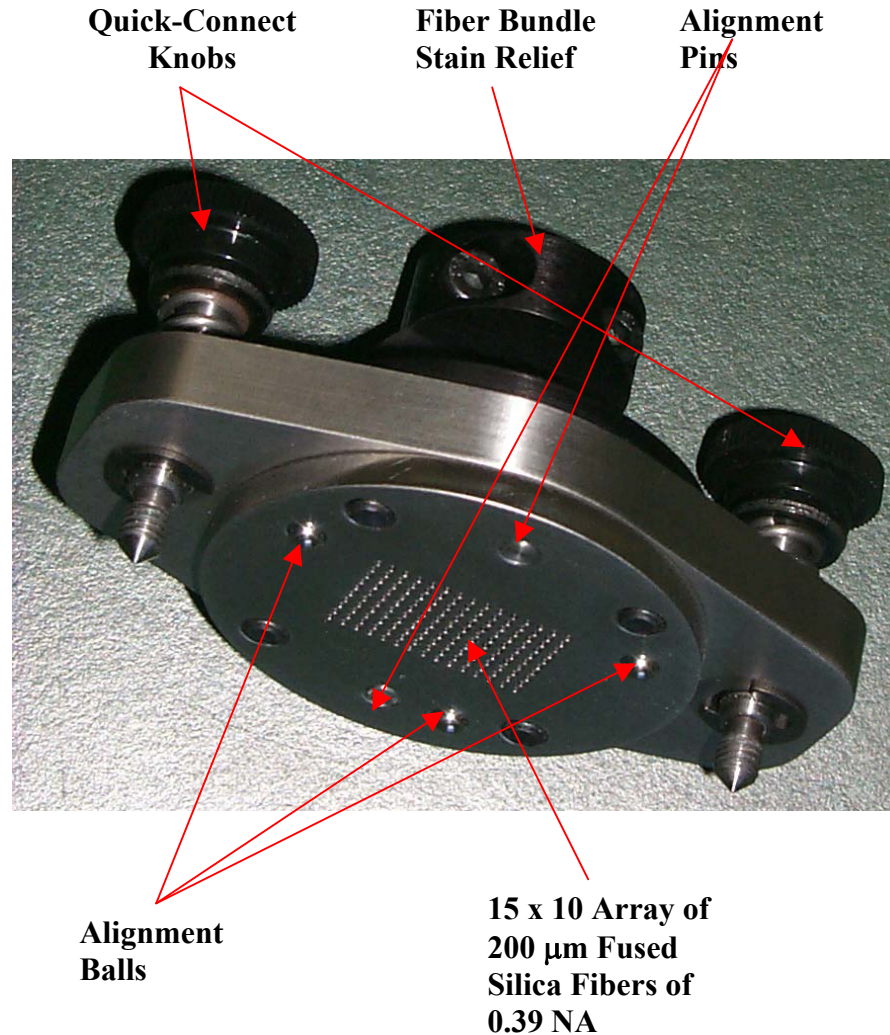
Figure 45   The Source Fiber Array Quick-Connect is shown. A 15 x 10 array of individually ferruled 200 μm diameter core fused silica fibers are held in very precise positional tolerance by kinematic mounting features. The knobs allow the connector to be quickly removed or attached with a positional repeatability within 5 μm.

telecentric scan lens. It was chosen over the 0.22 NA all-fused silica fiber due to cost

considerations and insensitivity of the temporal dispersion in transmitting through the 4

meters of source fiber. The very low NA (0.01) of the scan lens rendered the temporal

dispersion within the source fibers to be under 10 psec over a 4-meter length, which was

deemed insignificant. Thus, there was no benefit to using graded index fibers on the

source side. The fibers were individually ferruled and positioned within a 10 x 15 array

on 1.5 mm centers as shown in Figure 4.5. The ferrules were held in the assembly by a

silicone compression pad that held the ferrules tightly in the assembly upon compression

by the three lock-down screws. This allowed the individual fibers to be replaced in the

event of a broken fiber. A C-shaped collar provided strain relief against the black-

jacketed fiber bundle. The three ball bearings indicated in Figure 4.5 interfaced to

kinematic groves in the mating block within the Multiplexer, providing a positional
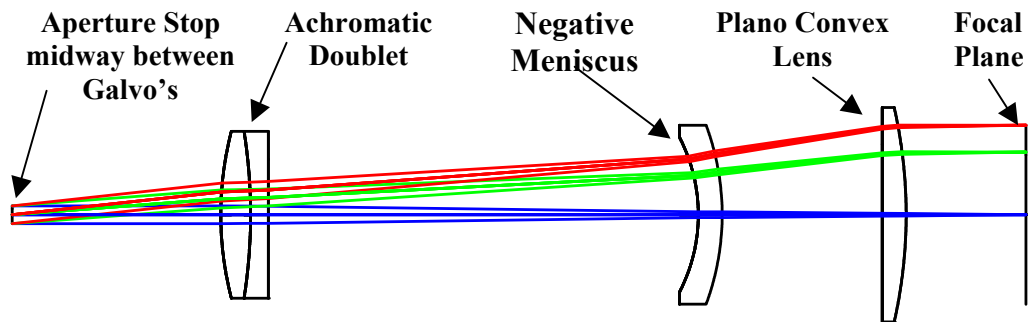
Figure 4.6   The Telecentric f/Theta scan lens that resides within the Multiplexer is shown. The
lens system is chromatically corrected over wavelength range between 650 and 1000 nm. The focal
plane field is 30 mm in diameter.

repeatability to within 5 μm. This eliminated the need to recalibrate the positions of the

fibers each time the source fiber array was removed and re-inserted. The two knurled

knobs allowed the Quick-Connector to be attached or removed within seconds.

The layout of the Multiplexer's telecentric scan lens is shown in Figure 4.6. The lens

system's aperture stop was positioned midway between the X and Y galvanometer

mirrors. The extent of the laser beam was on the order of 3 mm (approximately 2 mm

beam waist). The blue ray bundle of Figure 4.6 would correspond to fiber positions on

axis, the green rays to 70% of the field, and the red rays to a fiber at the edge of the field.

The lens was designed to accommodate an image field of 30 mm in diameter. The

prescription of the lens system is proprietary to the author's company, Innovations in

Optics, Inc., and will not be shown. The basic layout and performance data, however, are

shown below. The first lens group consisted of an achromatic doublet that balanced

chromatic aberrations against those induced by the last two elements. High index

materials were used to reduce coma, astigmatism, and spherical aberrations. The lens

was designed to be achromatic over the spectral range from 650 to 1000 nm. It was also

designed to accommodate a 10 mm diameter aperture stop. In the event that smaller

diameter source fibers were desired, a three or four to one beam expander could be used
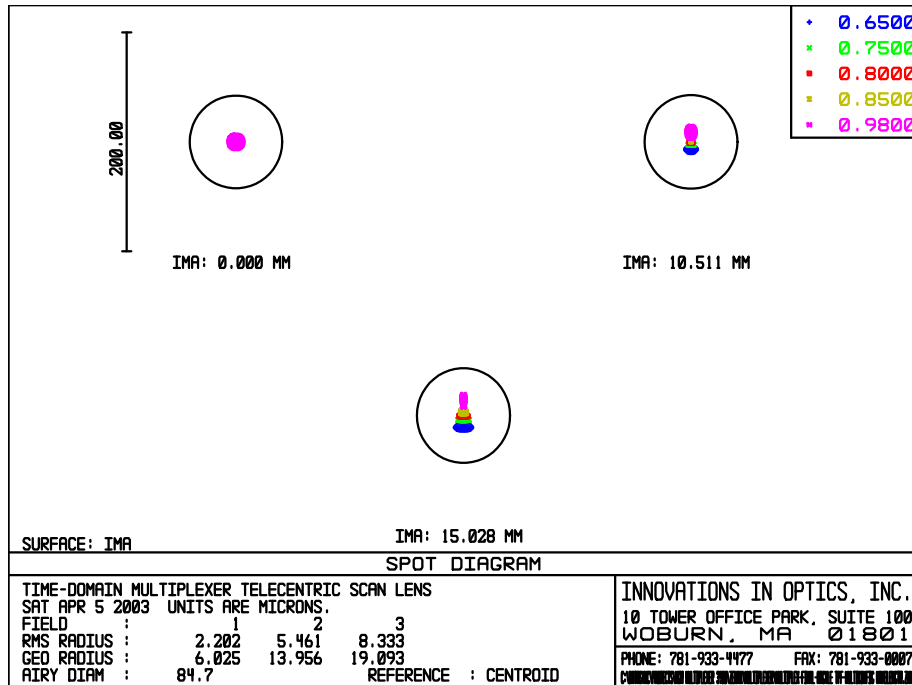
Figure 4.7   The Multiplexer scan lens spot diagram is shown for 3 field positions. The diffraction-limited Airy disk diameter is shown as 84.7 μm, indicating that the system is diffraction-limited for all field positions and all wavelengths.

to result in a smaller diffraction limited image. The third element consisted of a negative

meniscus lens, which worked in concert with the last element, a plano-convex lens, and

resulted in telecentricity in the image space. The telecentric condition was necessary to

assure that the central ray of each fiber input was aligned to the fiber axis. This assured

that the propagation through all fibers was as similar as possible. Strictly speaking, this was not necessary due to the t_0 fitting, but it is a good general practice.

It is clear from Figure 4.6, that the path length differences between the central and edge fiber positions caused a relative temporal shift on the order of a few psec, but again this is negligible and below the resolution of the system.

Figure 4.7 shows a spot diagram of the scan lens system for wavelengths ranging from 650 to 980 nm. The diffraction-limited Airy disk diameter is shown as a reference and had a magnitude on the order of 85 μm. A small degree of change in magnification with field, a parameter referred to as coma, is observed versus wavelength. This is also evident in the transverse ray fan plot of Figure 4.8 in the saggital (Y) plane for the two off-axis field points (10 and 15 mm). The geometric aberrations of the scan lens were small relative to the diameter of the Airy disk, thus this system would be referred to as a
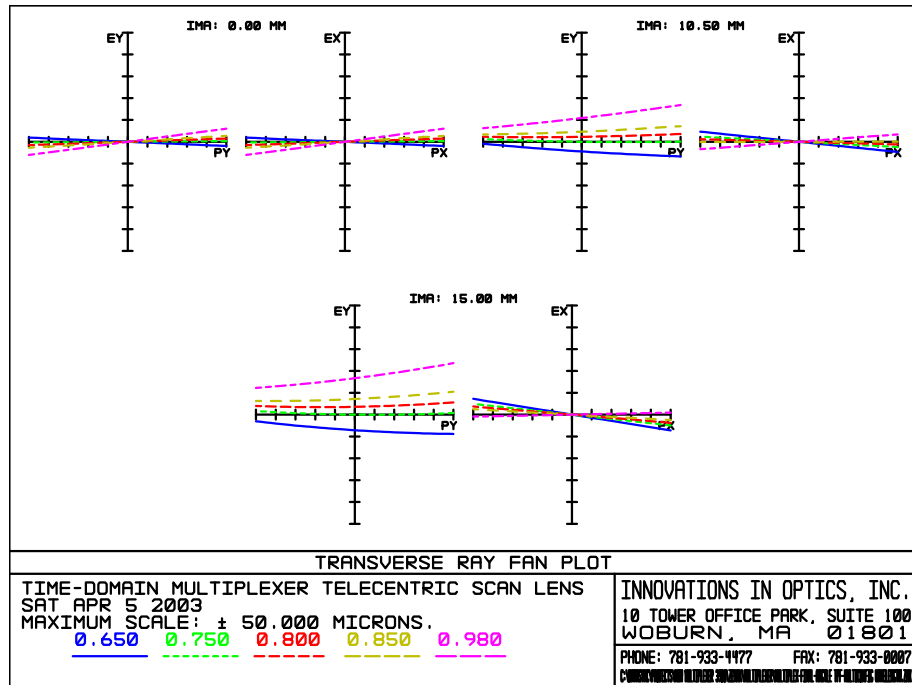
Figure 4.8   The transverse ray aberrations are shown for the Multiplexer scan lens for 3 field positions.

diffraction-limited lens system. This is also evidenced by the near diffraction-limited

performance of the polychromatic diffraction modulation transfer function (MTF) shown

in Figure 4.9. The MTF indicates the contrast that would be expected in image space as a
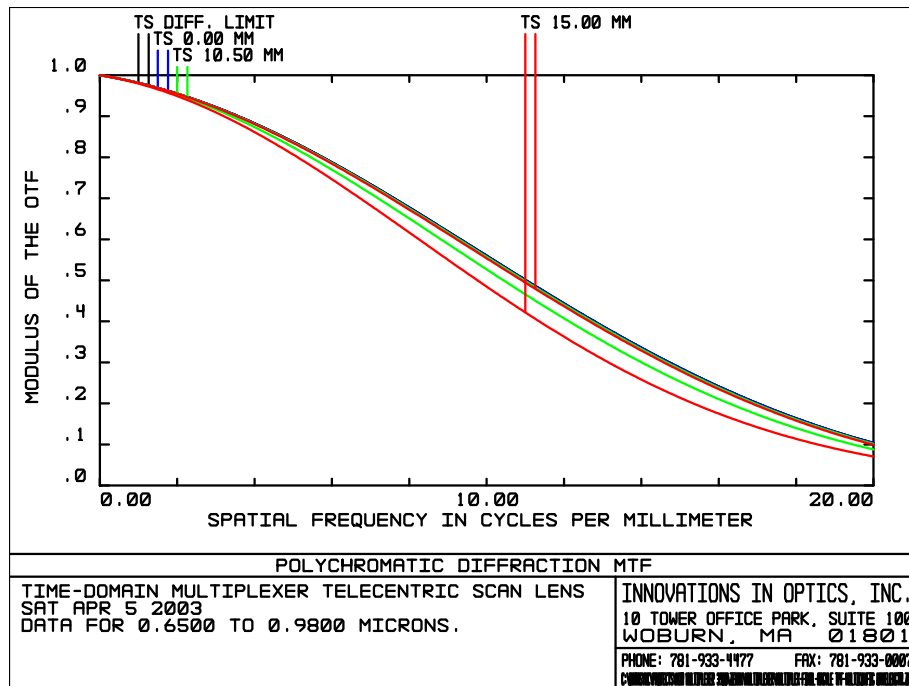
Figure 4.9   The polychromatic diffraction modulation transfer function (MTF) is shown for three fields, indicating the near-diffraction limited performance.

function of spatial frequency and represents a standard metric by which the optical

community assesses lens performance.

Figure 4.10 shows the polychromatic diffraction through-focus MTF of the scan lens

over a range of ± 10 mm. The MTF is assessed at 5 cycles per mm as a reference. The

plot indicates that the fibers had a depth of focus on the order of ± 2 mm, with negligible

effect on the MTF. This was a consequence of the very low image space NA of 0.01.

Figure 4.11 indicates that there was about 0.5 mm of field curvature due to

astigmatism at the edge of the field. The field curvature plot also indicates that there was

about 1 mm of focal shift between 650 and 980 nm, but this was well within the depth of
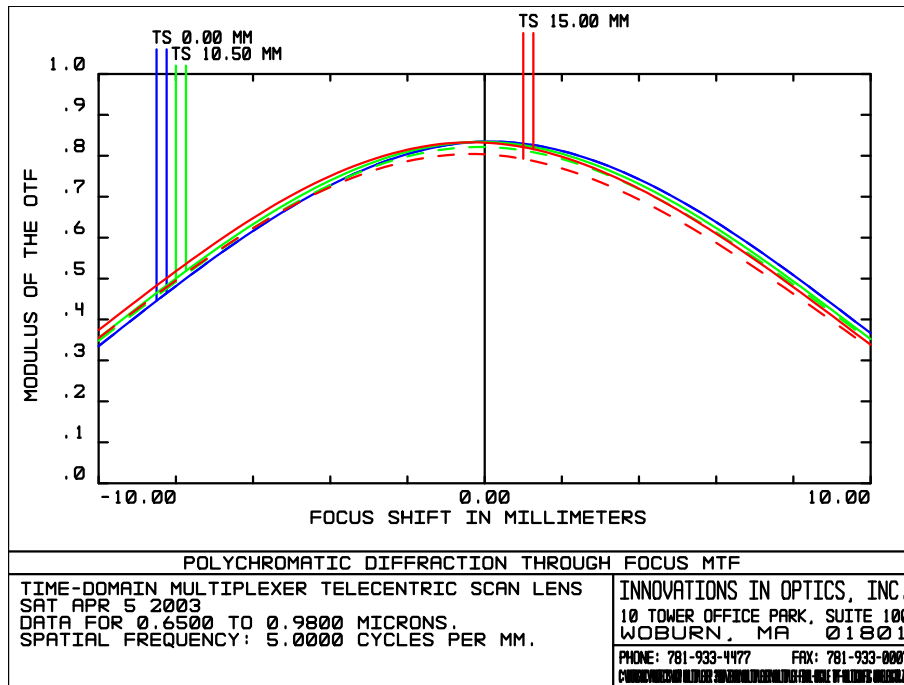
Figure 4.10   The polychromatic through-focus modulation transfer function (MTF) is shown for the Multiplexer scan lens for 3 field positions.
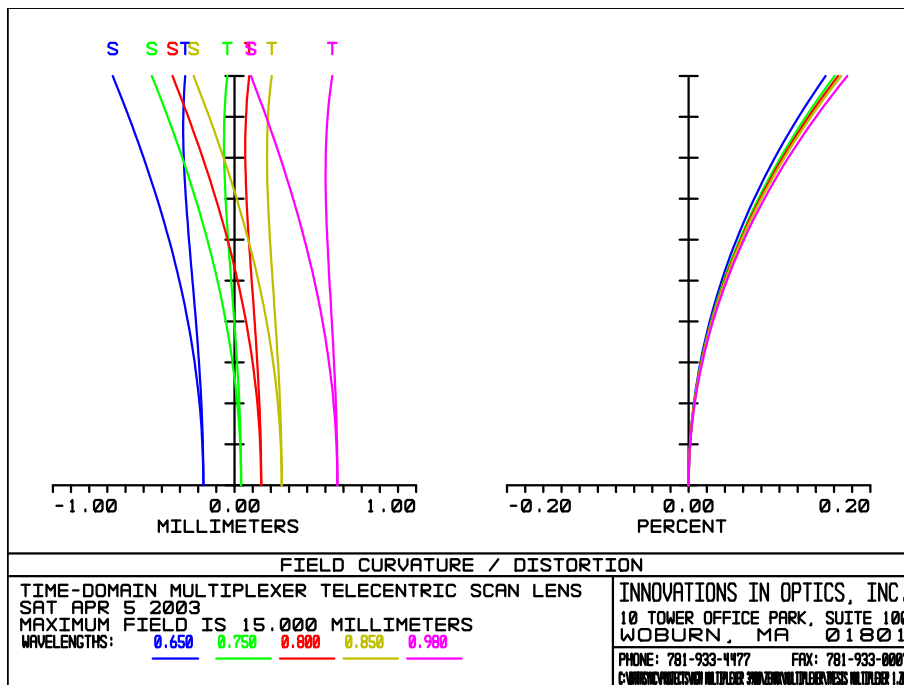
Figure 4.11   The field curvature and distortion is shown for the Multiplexer scan lens system plotted versus field.

focus limitations mentioned above. The distortion was held to an insignificant 0.2% at

the edge of the field. Absence of distortion in the image plane of the scan lens was not a strict requirement, as the galvanometer could be mapped to any position, but it did simplify the fiber position locating routines and assured that the acceleration profile from fiber to fiber was constant over the full field. In general, it is a good practice to minimize any difference the lens system may have on the launch conditions from fiber to fiber. Any of the lens system aberrations would become more important for the case of a larger aperture stop that would be used for smaller source fiber diameters. Given the high average power available from the laser, smaller source fibers could be used by rotating the polarizer to make up for coupling losses into smaller fibers, as limited by diffraction. Substantial reflections off the fiber ferrules, however, may produce unacceptably high cross talk between fibers due to retro-reflections off the lens elements.

Figure 4.12 shows an actual scan of the laser over one fiber near the center of the array and one near the edge of the array. The fiber diameter was 200 μm. The curves
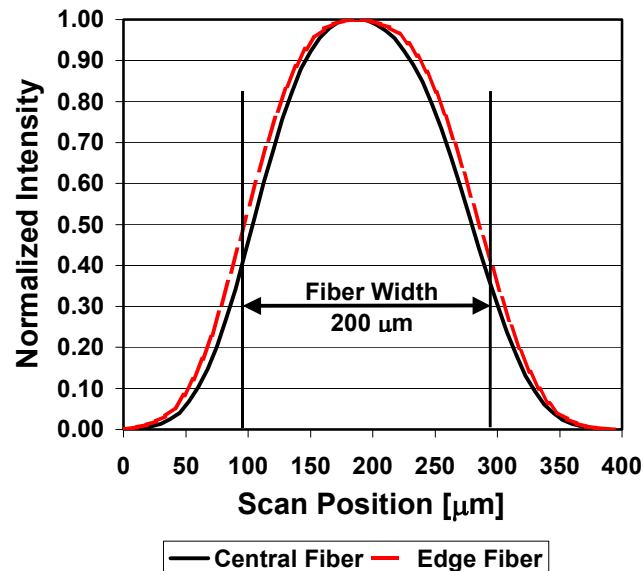
Figure 4.12   The normalized intensity is shown for the image of the laser scanned over a central and edge source fiber at a wavelength of 750 nm within the Multiplexer. The source fiber had a core diameter of 200 microns.

represent the convolution of the fiber aperture with the image of the laser. The curves

fall off within about 80 μm of the edge of the fiber diameter on both sides indicating the

diffraction-limited laser spot was consistent with that shown in the spot diagram of

Figure 4.7. The increased width at the edge fiber resulted from the slightly larger

aberrations at the edge of the field.

4.3   Time-Domain Detection Subsystem

The primary components of the Time-Domain Detection Subsystem are indicated in

Figure 4.13. The fiber bundle of 313, 400 μm diameter core, plastic-clad fused silica

fibers of 0.39 NA, is shown interfaced to the left side of the objective lens. The custom,
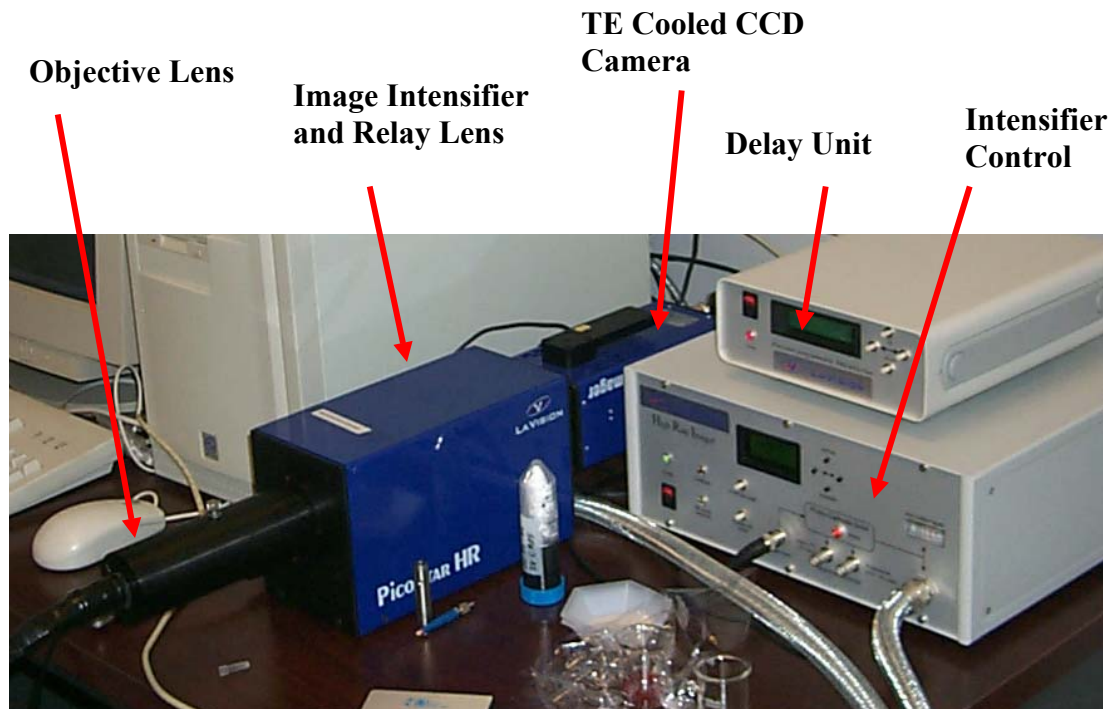
Figure 4.13   The gated, image-intensified CCD (ICCD) system is shown. The PicoStar HR
housing contains the time-gated photocathode, microchannel plate (MCP) intensifier, and a 2:1
relay lens to image the intensifier output on the CCD. The custom 1:1 fiber-array imaging lens is
shown mounted to the front of the ICCD. The delay unit and intensifier control are shown on the
right.

unit magnification objective is shown attached to the image intensifier and relay lens box, which itself, was attached to the thermoelectrically (TE) cooled charged couple device (CCD) camera. The details of the operation of the image intensifier are covered in Chapter 5. The ICCD PicoStar HR system was manufactured by LaVision, of Goettingen, Germany. The array of fibers from the detection probe was imaged with unit magnification to the photocathode of the image intensifier. The photocathode was time-gated by application of a positive potential relative to the front face of the intensifier, effectively turning its response on and off. This gate could be modulated at speeds up to about 1 GHz with a maximum duty cycle of 50%. The intensifier consisted of a proximity focused microchannel plate (MCP), which provided electron amplification of the photoelectrons ejected from the photocathode. The resulting cascade of electrons excited a phosphor at the proximal end of the MCP. The phosphor signal was then imaged by a 2:1 relay lens within the LaVision housing, onto the CCD camera. The laser operated at 80 MHz, which was much faster than the response of the CCD. Thus, the CCD was simply acting to integrate the signal that was in phase with the particular gate delay. The gate was delayed with respect to the time of incidence of the laser pulse on the tissue or tissue phantom. The gate control electronics are shown on the lower right of Figure 4.13. The controller allowed the selection of the gate voltage, the trigger mode, trigger offset, and gate width. The gate was adjustable in width between about 200 and 1000 psec, although it was found to be unstable for gate widths under 600 psec. Thus, all the work in this dissertation was done at a gate width of 600 psec. Also shown in the top right of Figure 4.13 is the gate delay controller, which could be adjusted by the computer. The time required to switch the delay was on the order of 500 msec.

The high performance, wide field, objective design shown in cross-sectional view in

Figure 4.14 enabled all 313, 400 μm diameter fibers to be imaged onto the photocathode.

The highly specialized optical design provided excellent performance over the full 18

mm diameter field of the photocathode. The lens system was chromatically corrected and

anti-reflection coated over the spectral range between 650 and 980 nm. With reference to
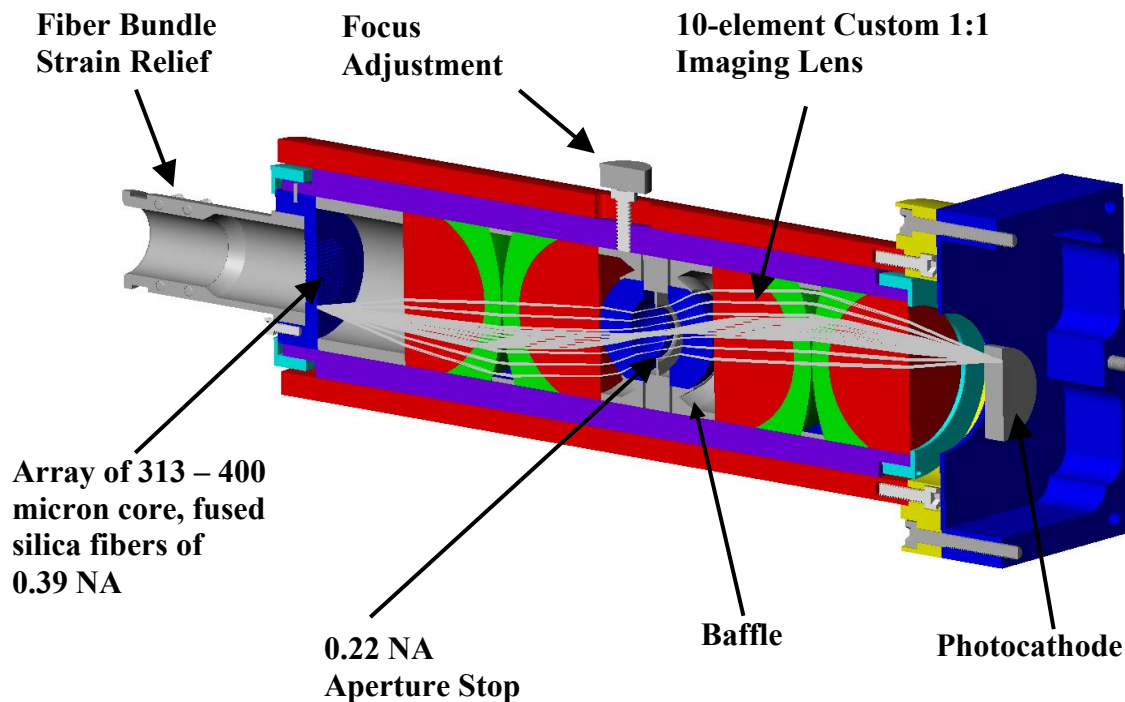
Figure 4.14   The custom designed 10-element 1:1 magnification bi-telecentric fiber array imaging lens is shown in a cross sectional rendered view. A total of 313 detector fibers of 400 micron diameter are imaged onto the photocathode.

Figure 4.14, the fibers were held secure by the fiber bundle strain relief and epoxied into

the fiber array holder, indicated in blue. All fibers were polished simultaneously, as the

fiber array holder comprised a portion of the fiber-polishing fixture. A ray bundle is

shown in gray for one fiber, indicating how the rays progressed through the optical

elements. There were a total of 10 optical elements, comprising 4 identical achromatic

doublets and 2 identical singlets arranged around a central stop. This was the best design

approach, as the symmetry about the centrally located stop caused many of the on-axis aberrations to cancel [1,2]. It would have been simpler to allow all the lenses to optimize to unique radii and thicknesses, but following good design practice, they were forced to be identical to minimize production costs.

A unique radiation trap baffle was designed to minimize stray light through the system. The baffles also acted as lens holders for the two singlets. The aperture stop limited the NA to 0.22, which was quite high for such a wide-field system. The fibers on the detection side were also the lower cost plastic-clad fused silica fibers, so it was important to assure excellent extinction of rays outside the NA of the lens system. The
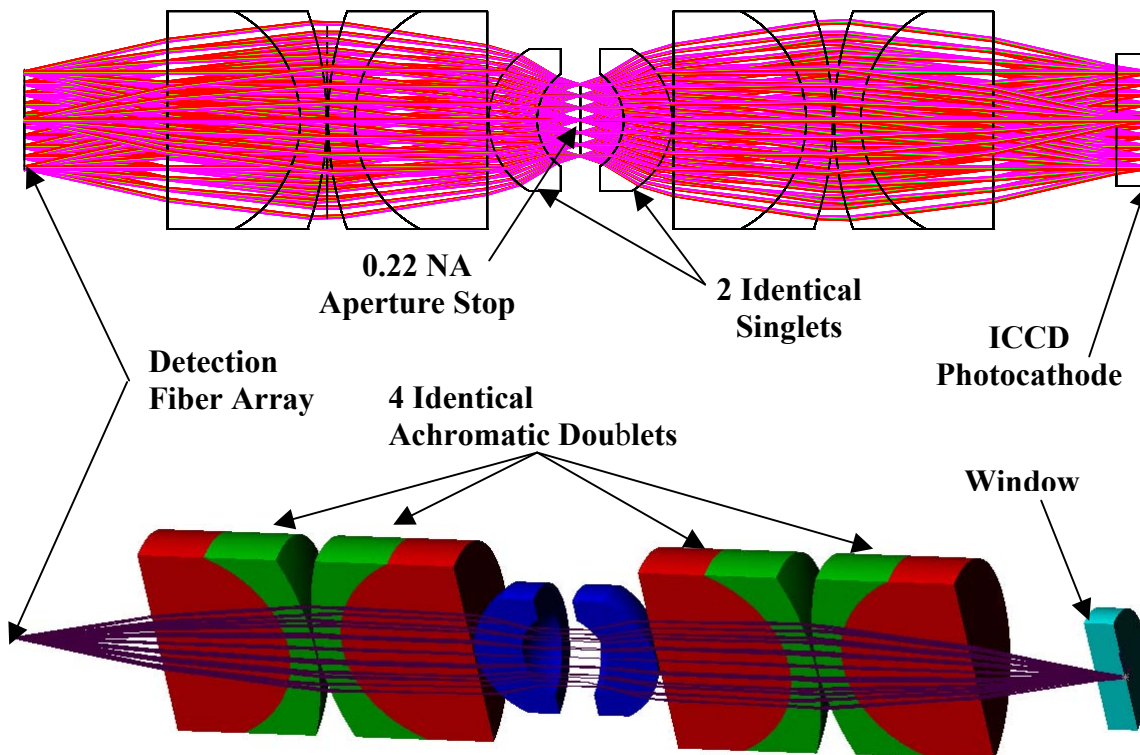
Figure 4.15   The ICCD camera objective is shown in cross section on the bottom and in 2-dimensional view on the top.

ratio percent of light passed by the system to that entering through the fibers was 30%. The excellent cross talk performance of the system discussed in the Chapter 6 is a testament to the efficacy of the baffle design.

The objective lens was housed in a tube that provided a means of focus adjustment. The lens was attached to the ICCD housing by four bolts. All hardware components were black anodized to cut down on stray light.

Figure 4.15 shows a cross sectional view in-plane on the top and in-perspective on the bottom of the objective lens system. The top view shows the extent of all the rays from all fibers. Again, this design is proprietary to Innovations in Optics, Inc., thus detailed prescriptions for the individual lens elements are not shown. The performance is indicated, however, in the plots below. There is sufficient space between the fiber array at the input and the first doublet to include one or more interference filters to minimize background from ambient light. The data collected in support of this dissertation, however, did not use a blocking filter. The performance of the system would not degrade
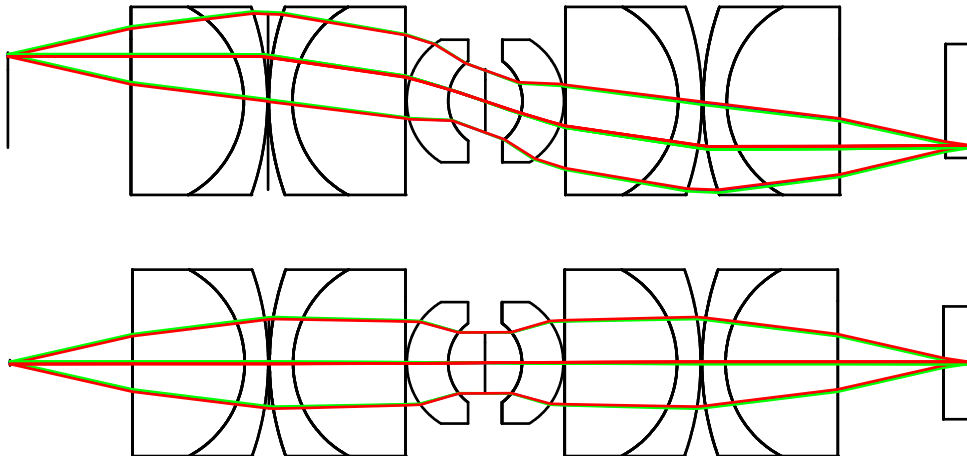
Figure 4.16   The ICCD 1:1 magnification Detection Fiber Array Imaging Objective is shown for a fiber on the edge of the field in the top view and for a fiber in the center of the field on the bottom view. The central stop limits the numerical aperture to 0.22.

from inclusion of a filter, in fact, it would improve just slightly, as the addition of a window near the fiber array would increase the system's symmetry due to the window in front of the photocathode.

Figure 4.16 shows a comparison of ray bundles for a fiber at the edge of the field (top view) and a fiber at the center (lower view). The lens system was telecentric in both object and image space. This helped minimize distortion that would have resulted for small defocuses for such a fast lens system. This was important because otherwise, the pixel map corresponding to detector fiber positions in the CCD image file would change as a function of focus.
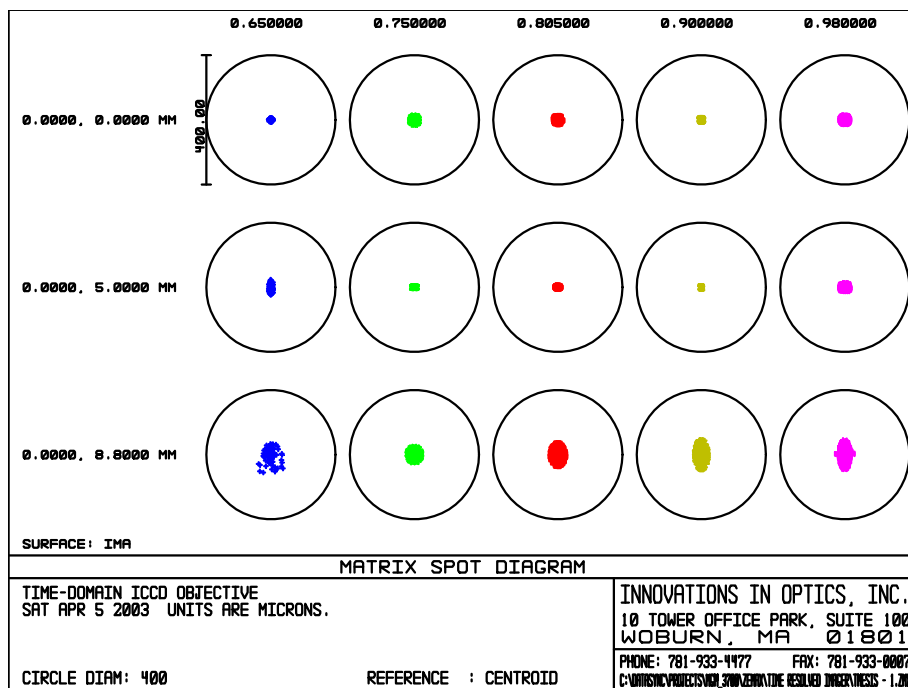
Figure 4.17 The spot diagrams for the ICCD objective lens are shown referenced to a 400 μm diameter fiber for three field positions and wavelengths from 650 to 980 nm.

Figures 4.17 through 4.23 indicate the performance of the camera objective. Figure 4.17 shows spot diagrams for wavelengths ranging between 650 and 980 nm for three field positions; on axis, 5 mm, and 8.6 mm, representing the edge of the field. The circle

is a reference indicating the 400 μm size of the detection fiber relative to the geometric spot size. Clearly, the lens system performs well for this size fiber over the full spectral band and full field.

Figure 4.18 shows the transverse ray fan plot of the camera objective lens system. The primary on-axis aberrations were spherical aberration, indicated by the characteristic S-shaped curve and chromatic focal shift, indicated by the change in slope with wavelength. Slight amounts of astigmatism and coma are evidenced for the off-axis fields. The saggital plane at the edge of the field also shows some fifth-order spherical aberration.
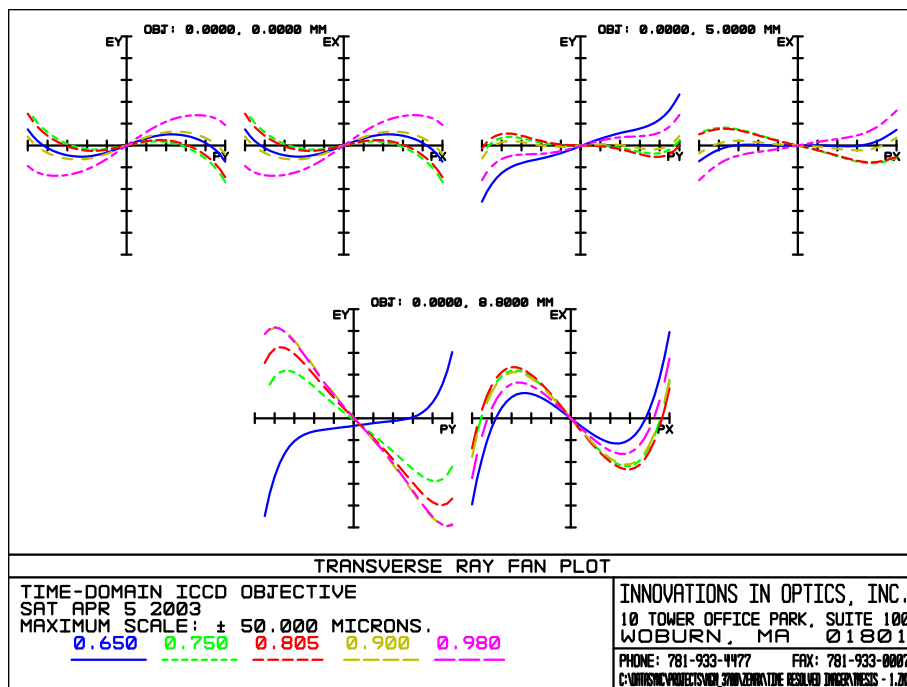
Figure 4.18   The transverse ray fan plot for the ICCD objective lens system is shown for three fields and wavelengths ranging from 650 to 980 nm.

Figure 4.19 shows the polychromatic diffraction MTF out to a spatial frequency of 20 cycles per mm, which would correspond to 25 μm between lines. The slight drop in
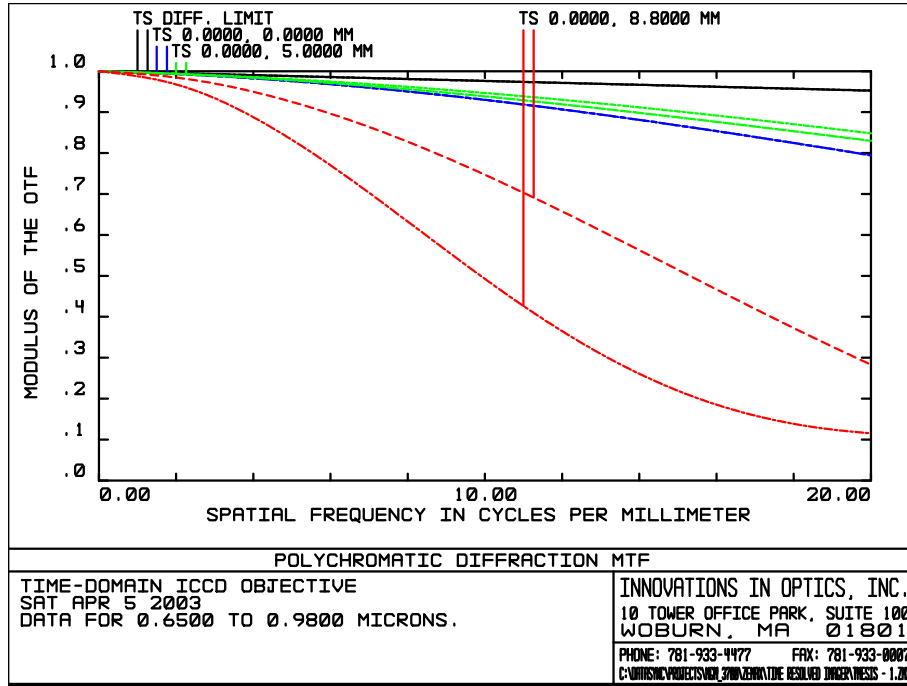
Figure 4.19   The polychromatic diffraction modulation transfer function (MTF) is shown for the ICCD objective lens system for three fields.
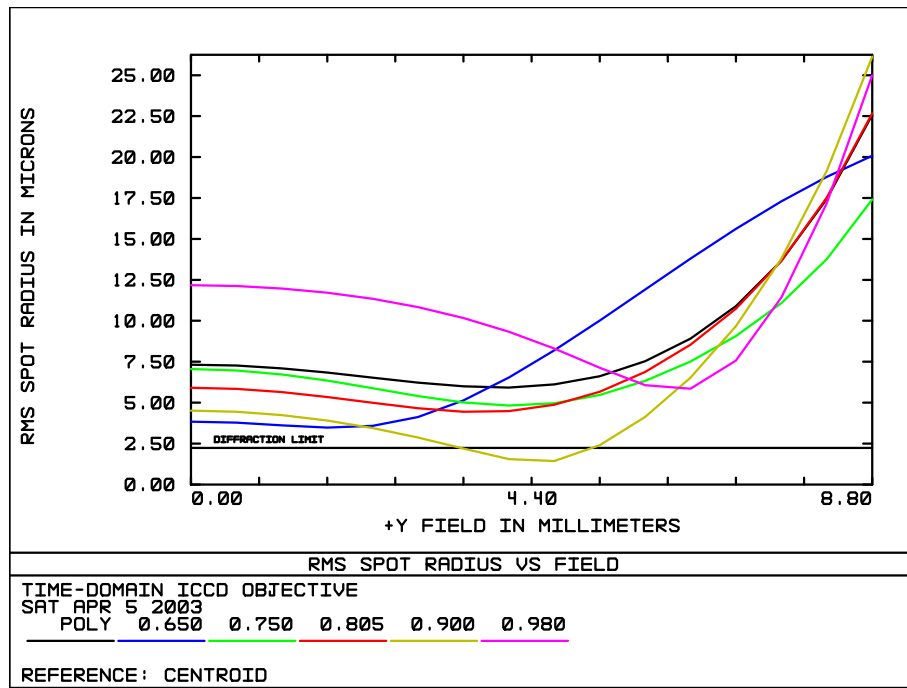
Figure 4.20   The rms spot radius versus field is shown for the ICCD objective lens system for wavelengths ranging from 650 to 980 nm.

performance at the edge of the field is evident, but it was still good relative to the

requirements of imaging a 400 μm diameter fiber with minimal blur.

Figure 4.20 shows the rms spot size in μm versus field. In general this lens system was not diffraction limited, as was the scan lens, but it did not need to be. Designing this lens for diffraction-limited performance over the spectral range, large field, and large NA, would not have been feasible. Any lens design represents many trade offs and it is important to keep perspective on the critical requirements.
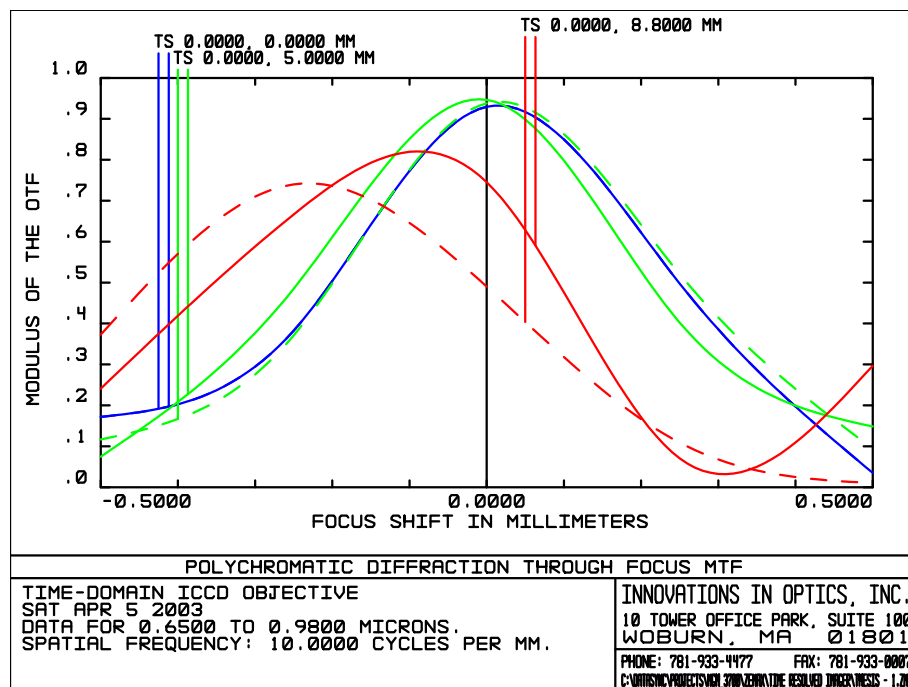
Figure 4.21   The polychromatic diffraction through-focus modulation transfer function (MTF) is shown to indicate focus sensitivity for the 0.22 NA ICCD camera objective lens system.

The lens system was very sensitive to focus due to the large NA as indicated in Figure 4.21 showing the polychromatic diffraction through-focus MTF. Focus had to be held to within a few hundred μm to maintain good performance. The shift in focus between the center field points and the edge of the field is also shown. Thus, the MTF of Figure 4.19 for the edge of the field could have been improved at the expense of

performance at the center of the field. In practice, the instrument operator would adjust the lens by eye. The edge of the field only applies to a handful of positions, so it is likely that the focus would be adjusted to be optimal closer to the center of the field. Focus adjustment was accomplished by slight movements of a lock-down knurled screw on top of the lens barrel. It may be useful for future versions of this system to have a more precise way to adjust focus, such as a rotating focus wheel that allows for greater focus resolution and control.

Figure 4.22 shows plots of field curvature and distortion versus field for the camera objective. The field curvature was the primary cause of decreased performance near the
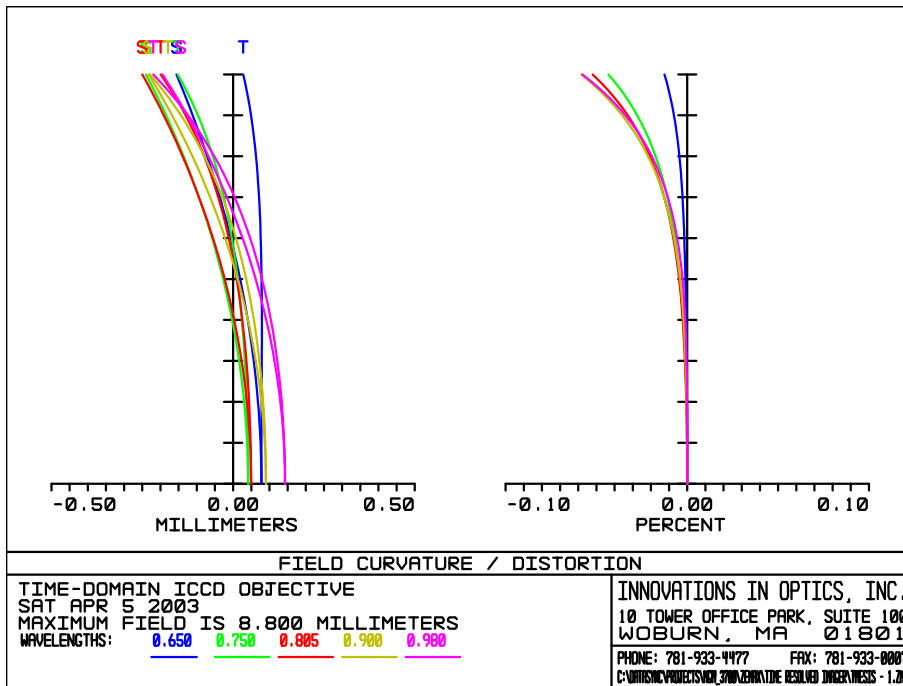
Figure 4.22   The field curvature and distortion for the ICCD objective lens system is shown for wavelengths ranging from 650 to 980 nm.

edge of the field. The distortion was held to well under 0.10% at the edge of the field. This was deliberate, as if the design had not been constrained to minimize distortion, it could have been as much as 10 to 15 % at the edge of the field. Many systems do have

significant distortion, such as endoscopes, or wide field camera lenses. For this system, however, low distortion meant that all fibers would map onto an equal number of pixels and the distance from center to center of the detection fibers on the image file would be uniform. This simplified calculations considerably.

The last figure in this section, Figure 4.23, shows a binary image map of the detection fibers onto the photocathode, simulated in the ZEMAX software package from FocusSoft, Inc., used to design the lens system. Only the edge fibers and a cross through the middle are shown due to configuration limits in the software. All of the 400 μm fibers were well resolved with no evidence of spill over, or cross talk into adjacent fibers.


```
                            IMAGE DIAGRAM
TIME-DOMAIN ICCD OBJECTIVE              INNOVATIONS IN OPTICS, INC.
SAT APR 5 2003                          10 TOWER OFFICE PARK, SUITE 100
SCALE BAR IS 18.0000 MILLIMETERS.       WOBURN,  MA   01801
FIELD POSITION: 0.0000, 0.0000 MM
EFFICIENCY:  99.999%. TOTAL POWER: 1.000E+000 WATTS    PHONE: 781-933-4477    FAX: 781-933-0007
SURFACE: 25                             C:\DATASYNC\PROJECTS\MGH_3700\ZEMAX\TIME RESOLVED IMAGER\THESIS - 2.ZMX
```
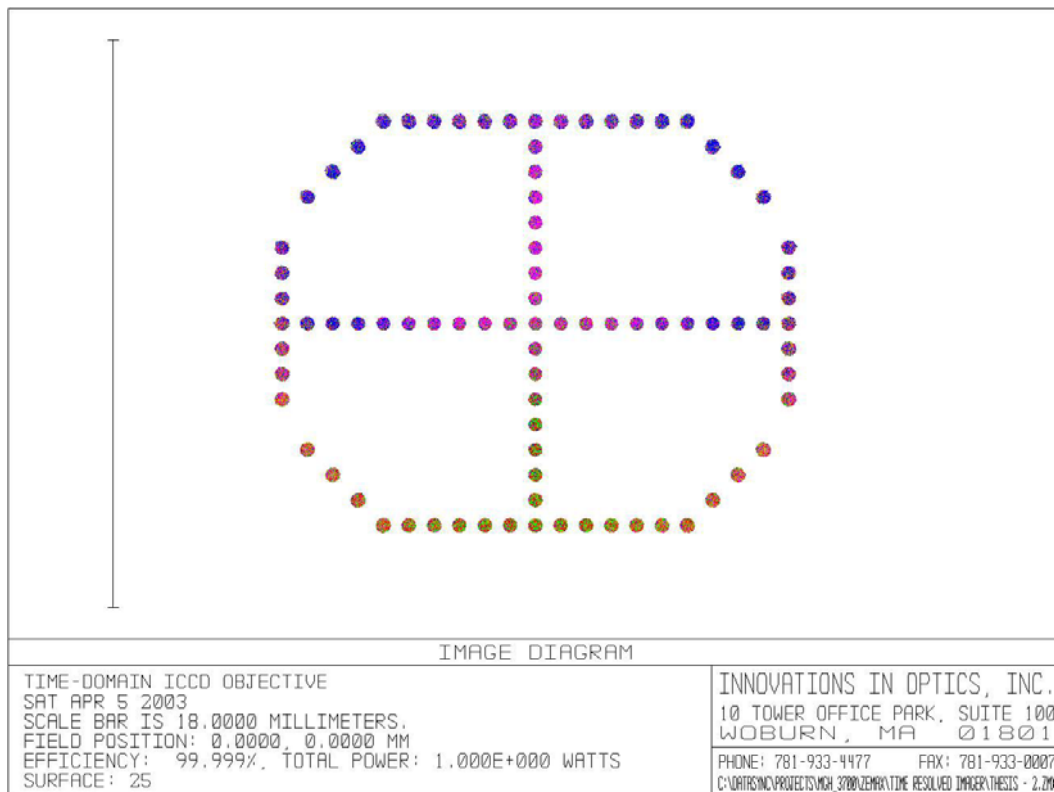
Figure 4.23   The image extent of the 400 μm diameter detection fibers is shown for the ICCD objective lens system. This result indicates that the lens system performs well for this application over the full field.

Only the four fibers at the top and bottom corners showed any sign of distortion. This

was due to the very nonlinear behavior of distortion at the edge of the field.

4.4 A Co-Registered Time-Domain Optical and X-Ray Mammography Probe

The basic architecture of the multi-modality Time-Domain Optical and X-Ray

Mammography Probe is shown in rendered view in Figure 4.24. An inverted modified
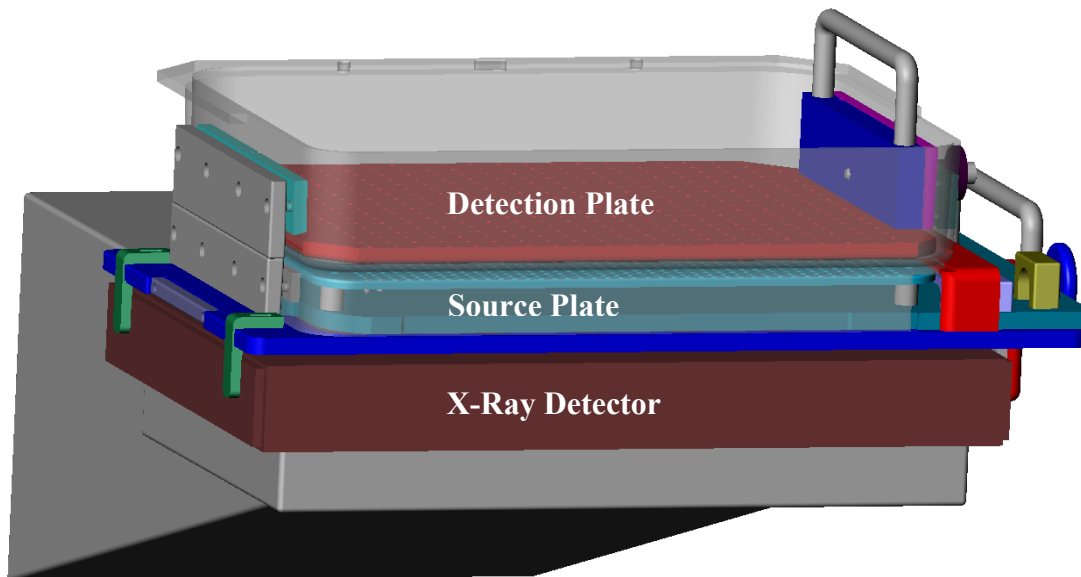
Figure 4.24 A rendered view of the source and detector probe assembly is shown interfaced to the X-ray detector of the X-ray digital tomosynthesis system. The source plate was positioned on the bottom within a modified compression plate. The detection plate was positioned on top within a second modified compression plate. An alignment bar assured precise positional accuracy between the two plates. Both the source and detector fiber plates had quick-release features to allow removal within seconds to permit the co-registered X-ray image to be acquired.

compression plate assembly was attached directly to the film box or detector of a

mammographic system. The source fibers were inserted into the compression plate to

allow laser pulses to be injected into the tissue. The top compression plate was also

slightly modified to accept a detection plate of fibers that collected a small fraction of the

scattered laser signal remitted from the breast tissue or tissue phantom. Both the source

and detection fiber plates were designed to be removed by quick release features to allow

for acquisition of a co-registered X-ray image within seconds of finishing the collection

of the optical data. The source plate had a knob that was turned by 180 degrees to allow

removal. The purpose of the rotating knob was to allow the fibers to slide by the

compression plate without scratching its surface. When the source plate was fully

inserted into the modified compression plate, the rotation of the knob caused the whole

source plate to move up against the inside of the compression plate to minimize coupling
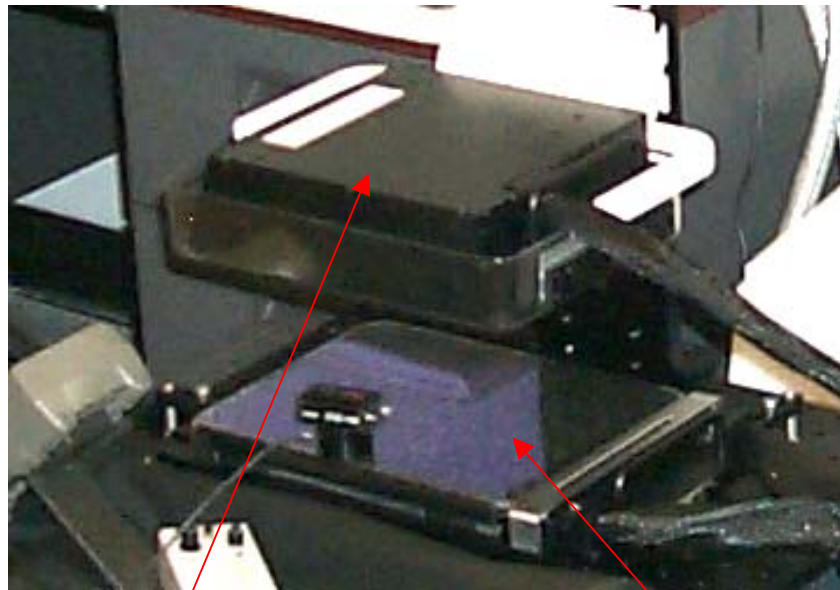
Detection Fiber Probe
Positioned within Modified
Upper Compression Plate

Source Fiber Probe
Positioned within Modified
Lower Compression Plate

4.25   The fiber optic source and detector probes are shown attached to the Phantom Stand.

from one source position to another.   The design and fabrication method for applying a

black mask to the surfaces of both the source and detector compression plates was

investigated. It was not done, however, due to budget constraints. The purpose of the

mask, that would have been comprised of a black layer applied to both sides of the

polycarbonate compression plates, except over the fields of view of the fibers, would have been to reduce coupling from one fiber position to another. The paints would not have represented contrast to the X-ray.

Figure 4.25 shows the source and detection probes mounted to the Phantom Stand
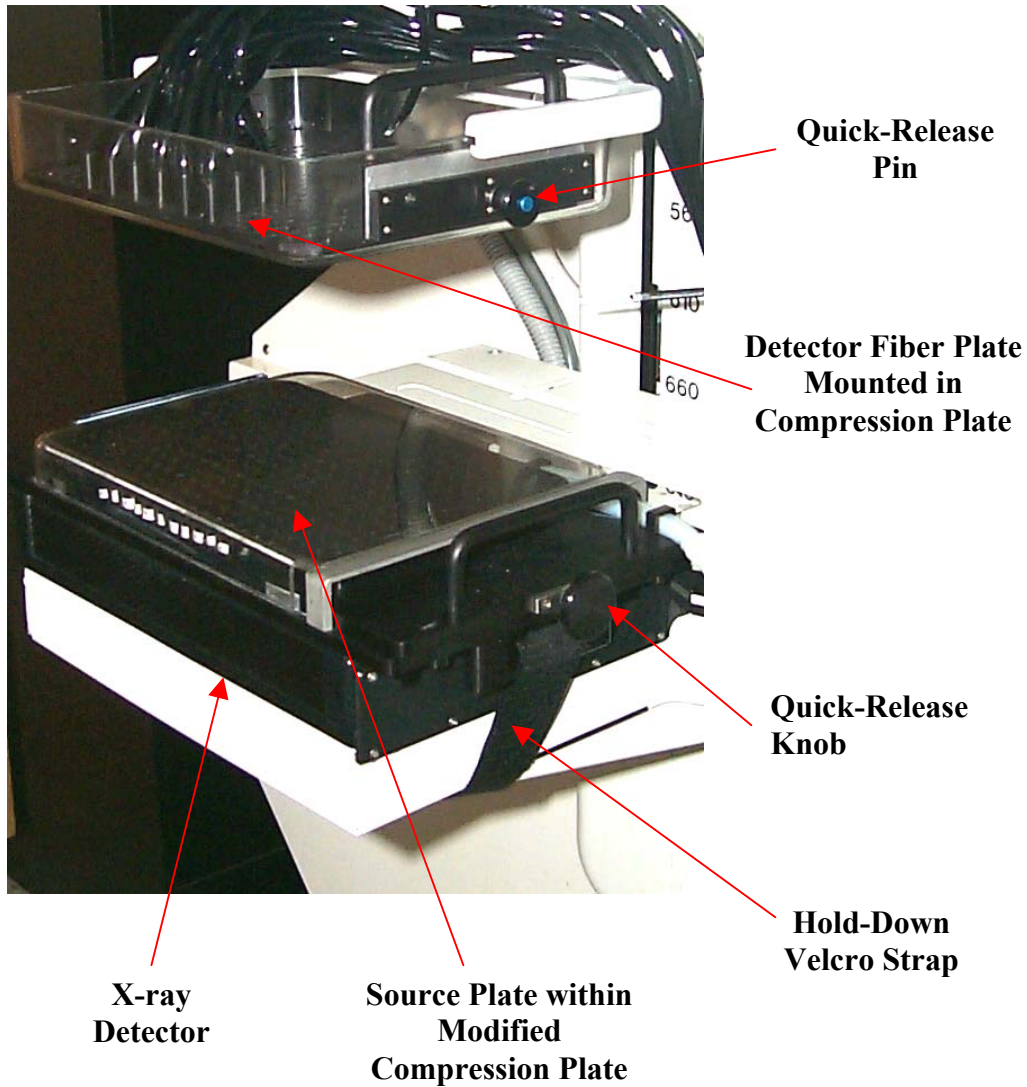
Figure 4.26   An early prototype of the source and detector probes are shown interfaced to an X-ray Tomosynthesis Mammography system. The source plate sits within a modified compression plate and mounts directly on top of the X-ray detector. The optical fiber detection plate sits within the upper compression plate. Both source and detector plates can be removed within seconds due to the quick release features to allow acquisition of the X-ray image following the optical data acquisition.

that is described in the next section. All exposed sides of both the source and detection probes were encased in metal to prevent damage to the fibers. All fiber bundles were strain relieved to prevent damage to the fibers.

Figure 4.26 shows an early prototype probe mounted to an X-ray digital tomosythesis system at Harvard's Massachusetts General Hospital, under the direction of Daniel Kopans, MD. The source probe on the bottom was mounted to the X-ray detector, and held in position by a Velcro strap. The quick-release knob on the source plate and the quick-release pin on the detection plate are clearly visible. The general procedure was first to compress the patient's breast between the compression plates and acquire an optical image within a period of about 2 minutes. Following the optical image, the source and detection plates were removed from their modified compression plates. The X-ray tomosythesis image was then acquired in co-registration with no movement of the patient.

A detailed view of the source detection plate is shown in Figure 4.27. The modified compression plate is shown on the right with the source fiber plate removed and sitting to the left. The compression plate assembly had two alignment slots to allow the source plate to be attached in two different directions to facilitate the measurement of medial lateral oblique (MLO) views, for which the source plate could not be removed in the direction of the patients shoulder.   The source plate had an array of holes on 5 mm centers to allow source fibers to be positioned in any desired pattern. This probe was actually a combined time-domain, RF, and CW probe, so it contained a total of several hundred individual fibers. There were two sets of 150 fibers that could be used for the time-domain system, one set at a time. The inset in the bottom of Figure 4.26 shows the

mechanism by which the ferrules were attached to the source plate. The ferrule was

positioned within the desired hole and then a small O-ring was placed over the tip of the

ferrule, locking it in place. The O-rings could be readily removed if desired, to allow

adjustment of fiber positions, or replacement, in the event of a damaged fiber.
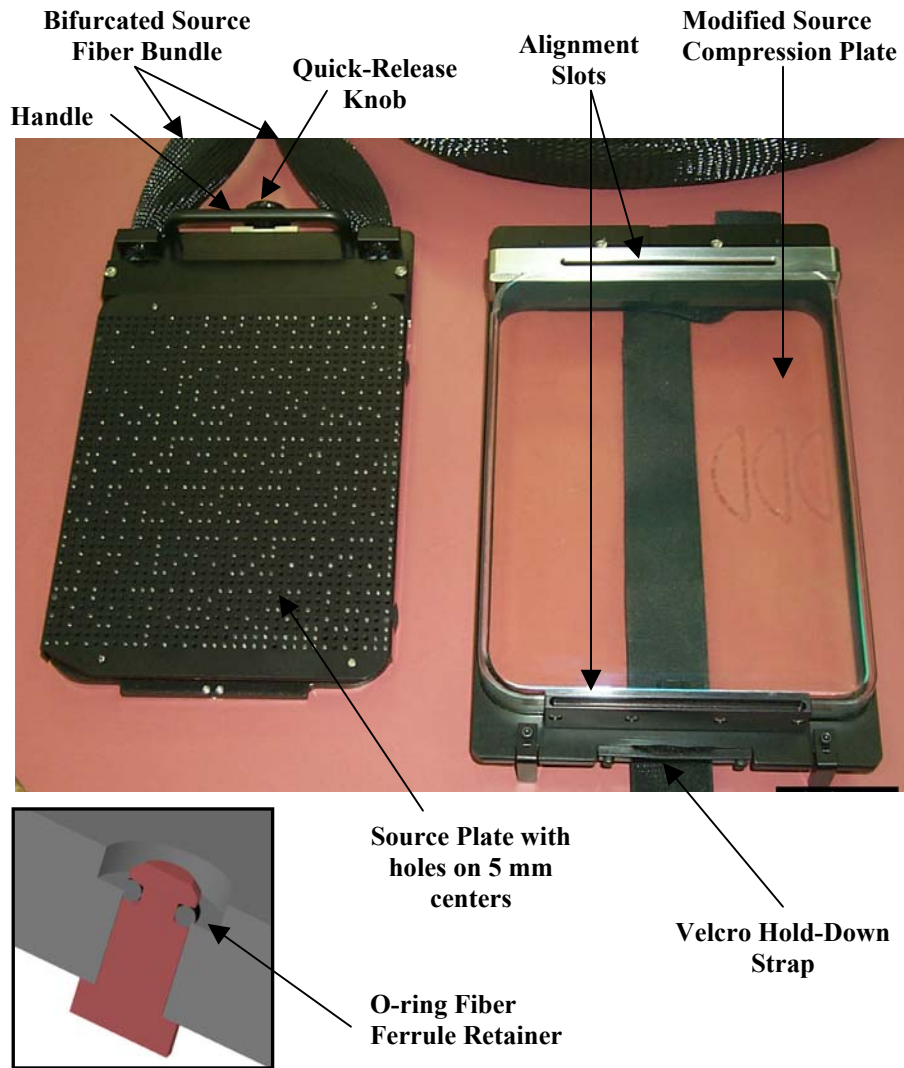
Figure 4.27   The quick-release source fiber plate and modified compression plate are shown
for the Time-Domain Breast Imaging System.

4.5   Phantom Design

Three phantoms were made to allow for system characterization as described in
Chapters 6 and 7. The phantom mold is shown in Figure 4.28. The dimensions of the
phantoms were 24 cm in length, 18 cm in width, and 6 cm in thickness. Two
homogeneous and one heterogeneous phantom were fabricated. The hollow fused silica
spheres, which comprised the heterogeneities, ranged in diameter from 1.5 to 2.5 cm.
They are shown suspended at various positions by 2 mm diameter ID silicone tubing.
The silicone tubing for each sphere was separate to allow either dependent or
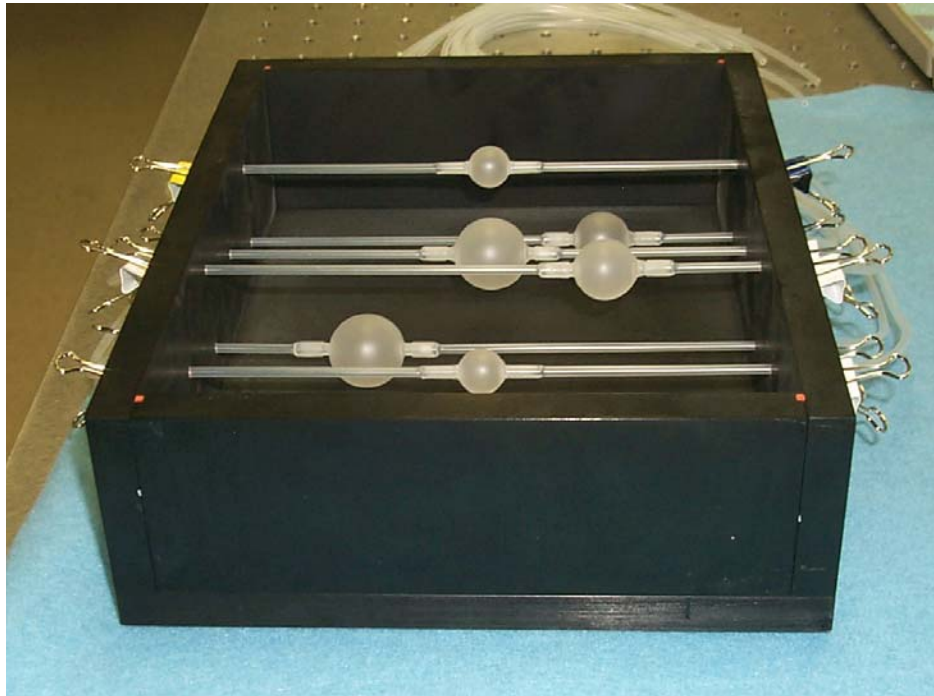
Figure 4.28   The 24 x 18 cm by 6 cm thick phantom mold is shown. The mold was used to
make both homogeneous and heterogeneous phantoms. The heterogeneities were comprised of
hollow fused silica spheres ranging from 1.5 to 2.5 cm in diameter, which were connected to the
outside and supported by silicone tubing. A suspension of TiO_2 particles and carbon black was used
in the silicone matrix to simulate typical background optical properties of breast tissue.

independent flow through the different spheres. The phantoms were made of a two-part
silicone elastomer (R-2615 from Nusil Technology of Carpinteria, CA) with a refractive

index n_d of 1.41, a pot life of 2 hours, a viscosity of 6000 cP, and a cure time of 2 hours at 65 Celsius. The elastomer was water clear over the full visible spectrum, even for several cm in thickness. The scattering was accomplished by the addition of TiO_2 (stock# 39953 with a 30 nm APS, from Alfa Aesar of Ward Hill, MA, 800-343-0660). The absorption

(A)

(B)
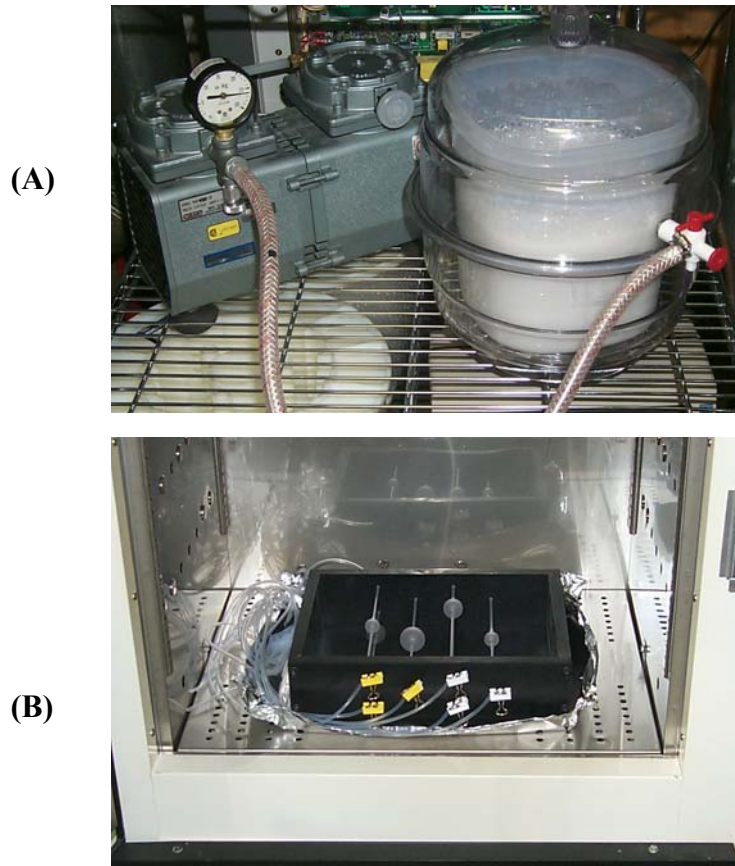
Figure 4.29   The vacuum system is shown in (A), which is used to pull the air out of the silicone after mixing in the $Ti:O_2$ and carbon black. About 30 minutes is required at 25 mm Hg vacuum. The heterogeneous phantom mold is shown in (B) within the oven ready for the silicone to be poured in. The phantom is cured in the oven for 2 hours at 65 Celsius.

was accomplished by the addition of carbon black (acetylene, 50% compressed, stock#39724 from Alfa Aesar). The carbon black extinction was determined by transmission through a standard 1 cm cuvette when mixed with part B of the silicone. The desired absorption was then obtained by titration. The TiO_2 was first mixed with the

balance of part B (100 cP), followed by 30 minutes sonication in an ultrasonic bath. All

ingredients were then combined in a 6-liter plastic tub and mixed thoroughly for 15

minutes. It was very important to pull all the trapped air out of the mix by placing the

entire tub in a large vacuum chamber; otherwise, unintended scattering could have been

caused by scattering from the trapped air bubbles. The mix was held at a vacuum of 25

mm Hg for a period of 45 minutes. The vacuum system is shown in Figure 4.29 (A).

Following air removal, the mix was carefully poured into the mold within the oven, as

shown in Figure 4.29 (B). A large glass plate was placed over the top and weights were

placed over the glass plate. Without the glass plate positioned on the top, the silicone

would have expanded in the middle, resulting in a non-uniform thickness. The phantom

was cured at a temperature of 65 Celsius for a period of 2 hours. The phantom was

allowed to cool slowly in the oven over a period of 30 minutes. The phantom mold had a

silicone mold release sprayed onto the black anodized walls and bottom to facilitate easy

removal.

The homogeneous phantom is shown in Figure 4.30 positioned between the source

and detector probes. The silicone tubes connecting the phantom were covered with

black tubing to prevent ambient light from coupling in through the tubes and to form a

complete black periphery around the outside of the phantom. A Phantom Stand was

constructed as shown in Figures 4.30 and 4.31 to allow the compression plate system to

be used in the laboratory environment. The relative positions of the phantom

heterogeneities can be seen in the rendered view of Figure 4.31.

**Compression
Plate Support
Attached to
Phantom Stand**

**Detection Fiber
Array Plate
with Cover**
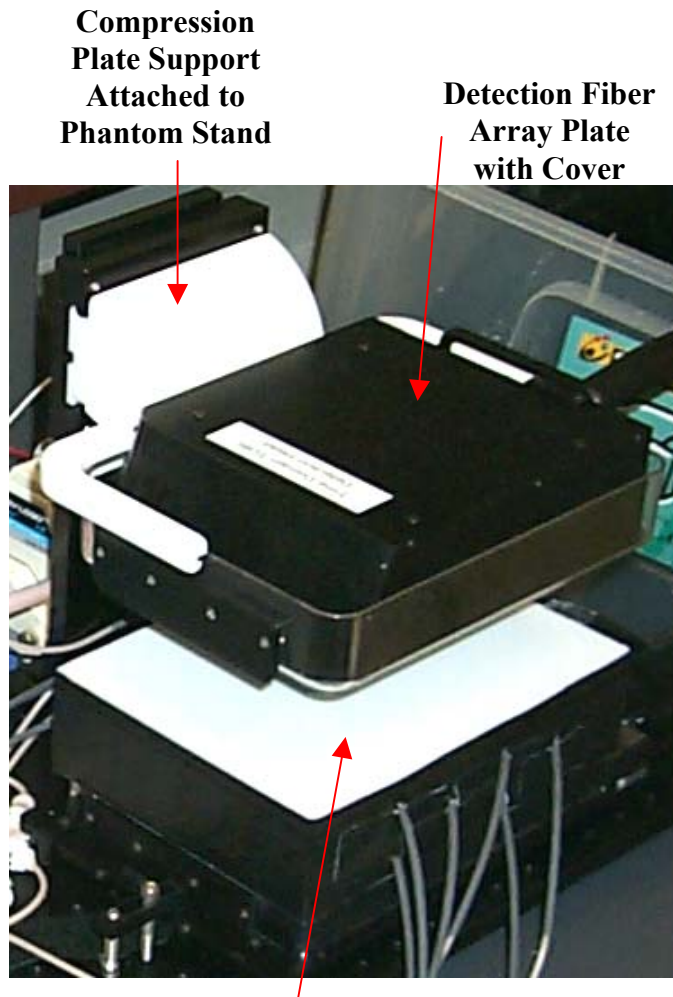
**Heterogeneous Phantom sitting on top of
Source Plate within Modified
Compression Plate**

Figure 4.30.   The Time-Domain Probe is shown attached to the Phantom Stand with the heterogeneous phantom positioned between the source and detector compression plates. The tubes out the side of the phantom are for fluid flow to the heterogeneities.
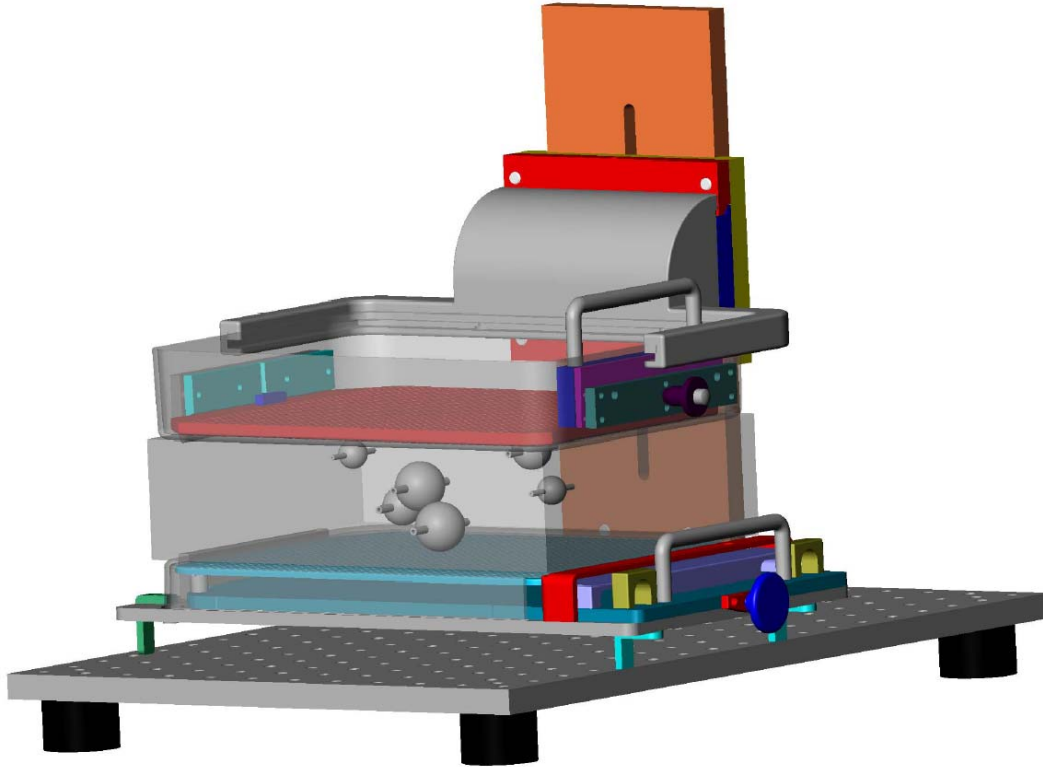
Figure 4.31   A rendered view of the Time-Domain Breast Imaging System Probe is shown attached to the Phantom Stand. The 24 x 18 cm by 6 cm thick heterogeneous phantom is shown positioned between the source and detector compression plates. The six hollow fused silica spheres can be seen positioned at various depths.

4.6   Summary

A unique and enabling Time-Domain Optical Breast Imaging System design was presented. Two important features of the design, aside from the use of a high average power and tunable laser, and a fast gated ICCD, were the extremely fast source fiber switching time of the Source Fiber Multiplexer and the high performance custom objective of the ICCD detection system. A quick-release multi-modality probe design was described that allowed for co-registration of optical and X-ray images. Also described were the design and fabrication of tissue phantoms.

Chapter 4 References

1. R. Kingslake, <u>Lens Design Fundamentals</u>, Academic Press, New York, 1978.
2. W. J. Smith, <u>Modern Optical Engineering: The Design of Optical Systems</u>, Second Edition, McGraw-Hill, Inc., New York, 1990.